Electronic Supplementary Material (ESI) for ChemComm.
This journal is © The Royal Society of Chemistry 2016

Lower critical solution temperature (LCST) phase behaviour of an ionic liquid and its control by supramolecular host-guest interactions

Shengyi Dong,[a] Jan Heyda,*[b] Jiayin Yuan[c] and Christoph A. Schalley*[a]

[a]*Institut für Chemie und Biochemie, Freie Universität Berlin,Takustrasse 3, 14195 Berlin, GermanyE-mail: c.schalley@fu-berlin.de.*

[b]*Physical Chemistry Department, University of Chemistry and Technology, Prague, Technicka 5, 16628 Prague 6, Czech Republic, Email: jan.heyda@vscht.cz*

[c]*Max Planck Institute of Colloids and Interfaces, Potsdam 14476, Germany.*

Electronic Supplementary Information (11 pages)

1. Materials and Methods

Materials: All materials were commercially available and used without further purification. **P5** was synthesized according to a literature-known method.[S1]

LCST phase behavior: UV/Vis absorption spectra were collected on a Lambda 950 UV/Vis/NIR spectrophotometer with a temperature controller and a cooling system. 1 cm quartz cuvettes were used. Cloud point temperatures were determined as the temperatures at which the transmittance at $\lambda \sim 550$ nm decreased by 50%.

2. Phase Behavior of IL-I in Different Solvents

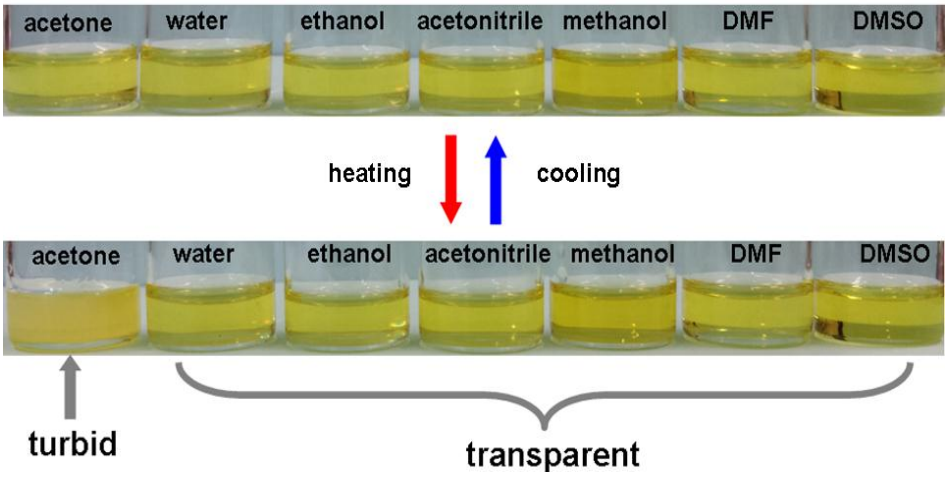

Figure S1. Thermo-responsive properties of **IL-I** in different solvents. The concentration of **IL-I** is 500 mg/mL for all samples. **IL-I** shows good solubility in all tested solvents and forms light yellow solutions at room temperature. Only the **IL-I**/acetone mixture shows LCST phase transitions upon heating to 50 ºC and cooling down back to room temperature. **IL-I** is not sufficiently soluble in hexane, toluene and ethylacetate to test its LCST behavior.[S2]

*3. ^{1}H NMR Spectra of **IL-I** in Different Solvents*

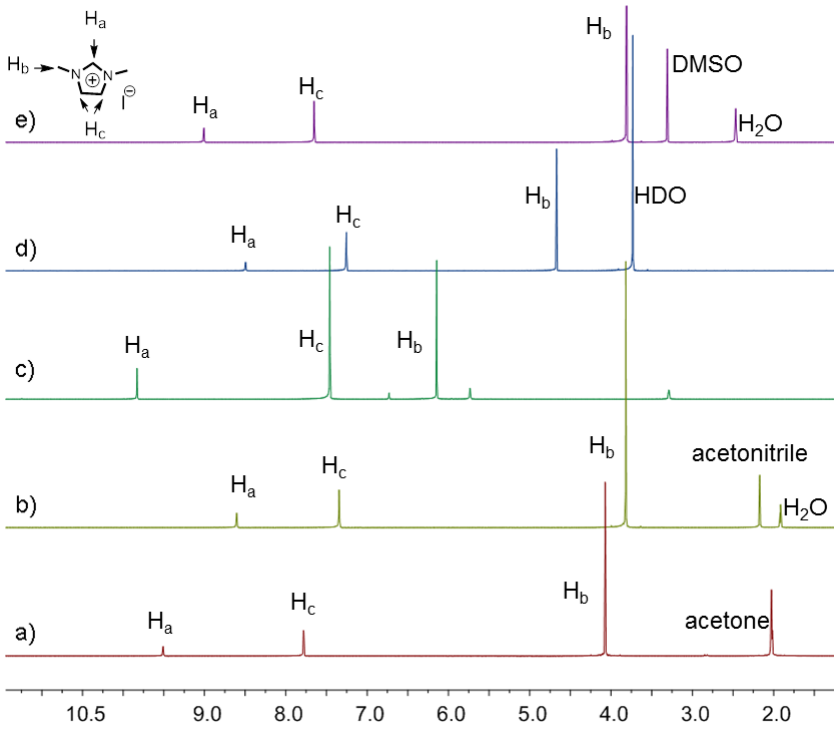

Figure S2 ^{1}H NMR spectra of **IL-I** in different solvents (10 mM, 298 K, 400 MHz): a) acetone-d_6; b) acetonitrile-d_3; c) ethanol-d_6; d) D_2O; e) DMSO-d_6.

4. Cloud Point Extraction (CPE) Experiments

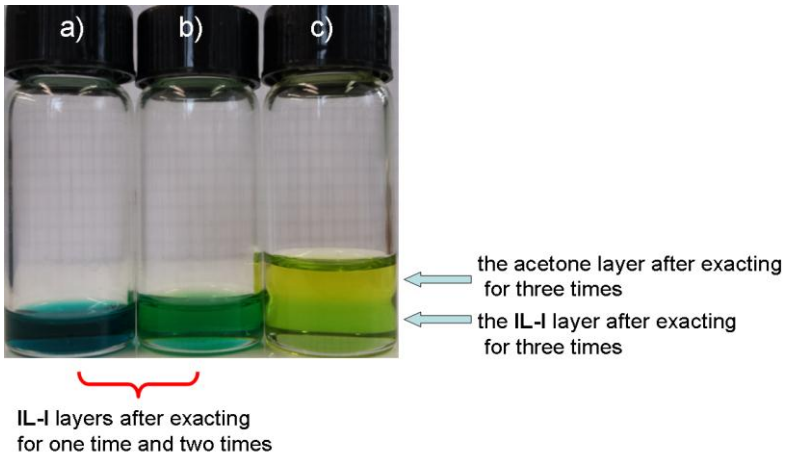

Figure S3. Photos of the CPE experiment: a) the **IL-I** layer after CPE for one time; b) the **IL-I** layer after CPE twice (new fresh **IL-I** is added to the acetone layer before the second CPE step); c) phase separation after CPE for three times: Only a small amount of azure A is still left in the **IL-I** phase. The color of the acetone phase indicates almost no azure A to be left.

5. Computational Methods

Molecular dynamics (MD) simulations of solutions containing a mixture of acetone and 1,3-dimethylimidazolium iodide or chloride were performed.[S3] The force fields of **IL-I** and **IL-Cl** were refined recently to account for charge transfer (the total charge of **IL** ions ~ ± 0.7), to be consistent with ab-initio calculations.[S3,S4] The acetone force field was taken from a recently developed solvent database.[S5]

Employing the Gromacs software,[S6] simulations were performed at three temperatures (300 K, 320 K, 340 K) at ambient pressure (101 kPa), which were controlled by a weak velocity rescale coupling scheme,[S7] and the Parrinello-Rahmann barostat,[S8] respectively. Electrostatic interactions were properly calculated by the particle mesh Ewald summation with standard cut-off (1 nm) and grid parameters.[S7] The integration time step in the simulations was 2 fs and statistics were gathered every 1 ps. After initial minimization, 20 ns of equilibration phase followed. Then the data were gathered in 80 ns production run, based on which converged radial distribution

functions for ions and solvent were obtained. To avoid finite size effects in solution structure, we studied relatively large systems with an equilibrium length of approximately 6 nm of the cubic and periodically repeated box (Figure S8).

Since the concentration effects are crucial during the demixing process, we also studied the system at different concentrations of ionic liquid; the system contained always 1000 acetone molecules, in which 35 **IL** molecules (about 60 mg/mL in the case of Cl^-, 110 mg/mL in the case of I^-), 220 **IL** molecules (about 410 mg/mL for the Cl^-, 700 mg/mL for I^- salt), or 375 **IL** molecules (about 690 mg/mL for the Cl^-, 1170 mg/mL for the I^- salt) were inserted. We note for clarity that concentration scale "mg/mL" refers to mg of **IL** added to 1 mL of acetone.

6. Analysis of Simulation Data

The MD simulations allowed determining the solution structure in terms of radial distribution functions, $g_{ij}(r)$, for species *i* and *j*. It is common and convenient to use index 1 for the solvent and 3 for the ionic liquid. In order to distinguish cation and anion, we used (+) for the 1,3-dimethylimidazolium cation and (-) for the counterion. In order to connect to macroscopic thermodynamics, we employed a theory of solutions,[S9,10] which relied on volume integrals of $g_{ij}(r)$, also called Kirkwood-Buff integrals, as defined in equation (S1)

$$G_{ij} = \iiint_{-\infty}^{\infty} \left(g_{ij}(\boldsymbol{r}) - 1\right) dV = 4\pi \int_0^{\infty} \left(g_{ij}(r) - 1\right) r^2 dr. \quad (eq.S1)$$

Several macroscopic properties can be easily derived from the Kirkwood-Buff integrals. For binary solutions these are partial molar volumes, isothermal compressibility, and activity coefficient derivative.[S10] The last one is the most sensitive measure of ion-ion and ion-solvent interactions and can be determined as a combination of G_{33} and G_{31} according to equation S2.

$$a_{33} = \frac{\partial \ln a_3}{\partial \ln c_3} = \frac{1}{1 + c_3(G_{33} - G_{31})} \quad (eq.S2)$$

$$B_2 = -2\pi \int_0^{\infty} (e^{-\frac{u_{eff}(r)}{k_B T}} - 1)\, r^2 dr \quad (eq.S3)$$

The second virial coefficient, Equation S3, is defined analogously to the KB-integral, and $g_{ij}(r)$ is replaced by $\exp(-u_{eff}(r)/k_BT)$.

$B_2(T)$ intrinsically varies with temperature, through temperature dependent effective potential $u_{eff}(r;T)$. Together with the 3rd virial coefficient (often approximated by hard-sphere form $B_3=2\sigma^6$, where σ stays for the effective radius of the particle), it can be used in a cubic equation of state (EOS, equation S4), out of which we may determine, via Maxwell construction, the spinodal and binodal curves and finally the critical temperature and density.[S11] In the EOS (eq. S4), c_3 is the density of **IL** in the bulk, P is the pressure, and $\beta = 1/k_BT$, where k_B is the Boltzmann constant.

$$\beta P = c_3 + B_2(T)c_3^2 + B_3 c_3^3 \quad (eq.S4)$$

We note that in our case, the solute-ionic liquid possesses charge, and thus the solution structure also varies with concentration, $g(r;c_3,T)$. Consequently, the effective potential contains a nontrivial concentration dependence, $u_{eff}(r;c_3,T)$, thus limiting the direct applicability of equation S4. To that end, we have performed direct MD simulations at different concentrations of **IL**, which provides us with two qualitatively different regimes as seen on examples of **IL** containing Cl^- vs. I^-. See Figure S4, and S5.

Three dimensional insight into ion-ion and ion-solvent interaction is obtained from spatial distribution functions (see below in Figure S6).

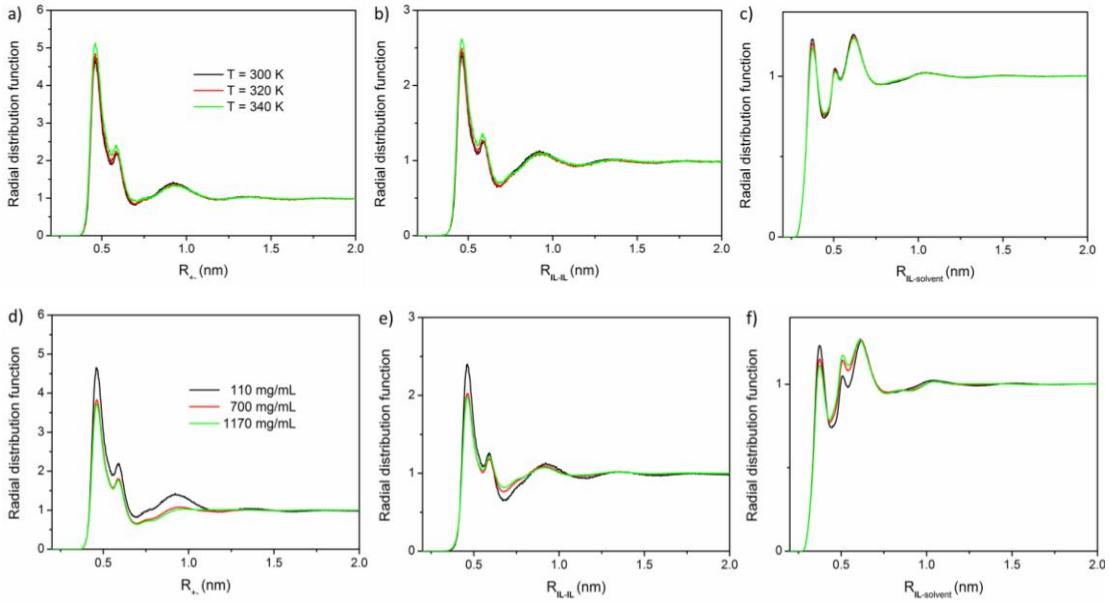

Figure S4. Radial distribution functions of **IL-I** in acetone, $C_{\mathbf{IL\text{-}I}}$ = 110 mg/mL) at 300 K (black line), 320 K (red), 340 K (green), respectively: a) the cation-anion distribution; b) the mean distribution of ionic liquid with ionic liquid; c) the mean distribution of the ionic liquid with acetone. Comparison of solution structure at a fixed temperature, T = 300 K, with concentration of ionic-liquid $C_{\mathbf{IL\text{-}I}}$ = 110 (black), 700 (red), and 1170 mg/mL (green), respectively: d) the cation-anion distribution; e) the mean distribution of ionic liquid with ionic liquid; f) the mean distribution of the ionic liquid with acetone.

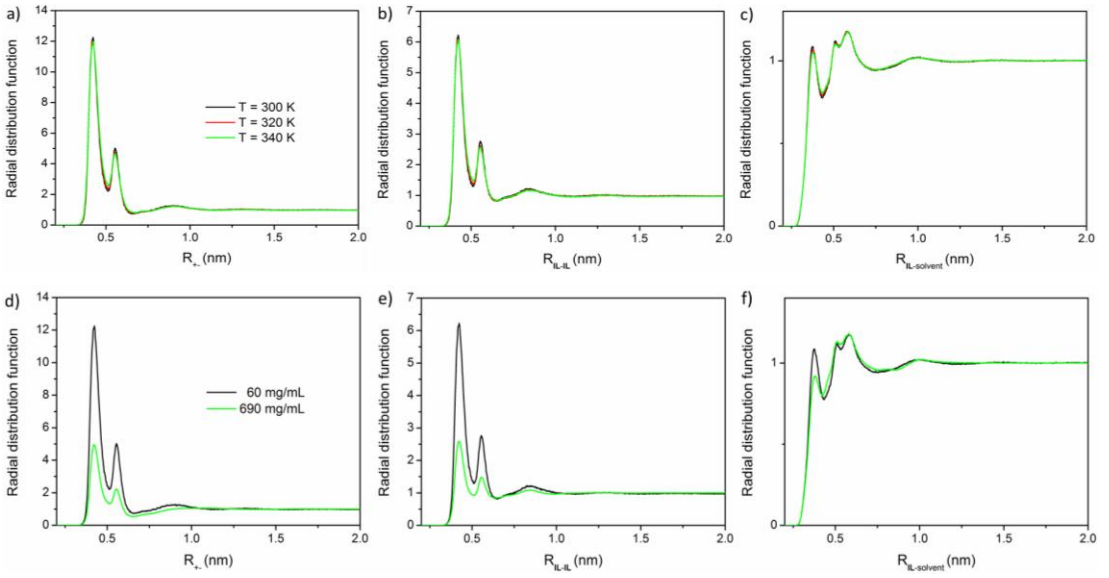

Figure S5. Radial distribution functions of **IL-Cl** in acetone, $C_{\mathbf{IL\text{-}Cl}}$ = 60 mg/mL) at 300 K

(black line), 320 K (red), 340 K (green), respective: a) the cation-anion distribution; b) the mean distribution of ionic liquid with ionic liquid; c) the ionic liquid with acetone on the right, respectively. Comparison of solution structure at a fixed temperature, T = 300 K, with $C_{\mathbf{IL\text{-}Cl}}$ = 60 (black) and 690 mg/mL (green), respectively: d) the cation-anion distribution; e) the mean distribution of ionic liquid with ionic liquid; f) the mean distribution of the ionic liquid with acetone.

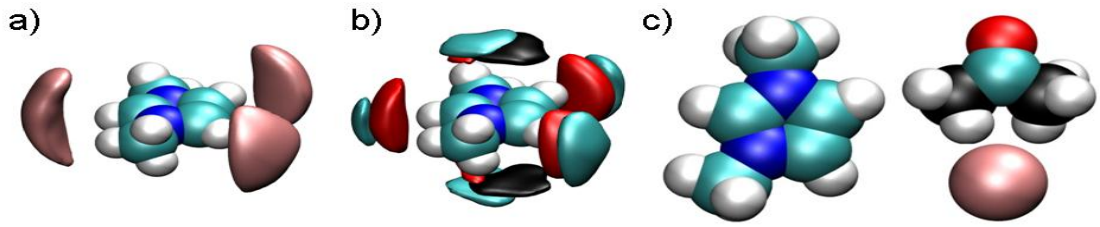

Figure S6. a) The spatial distribution of iodide (pink, density is presented for contour = 6, *i.e.*, 6x the bulk density of I^-) around the 1,3-dimethylimidazolium (blue for nitrogen, white for hydrogen and light cyan for carbon). We note that with lower probability (2.3x bulk density), the iodide can bind around the plane of the imidazolium ring; b) the distribution of acetone to the 1,3-dimethylimidazolium, where carbonyl oxygen is in red (3x), carbonyl carbon in cyan (3x), and methyl moieties in black (2.2x), respective; c) colors representing different atoms in studied molecules.

In order to gain further insight, we calculated for 1,3-dimethylimidazolium the spatial distribution of iodide and acetone. The results of this analysis are presented in Figure S6. It can be seen that negatively charged iodide is predominantly located in the plane of 1,3-dimethylimidazolium and near methyl groups, For these locations, there exists acompetition with the carbonyl oxygen atom of acetone (comparing spatial density location in 6a and 6b).

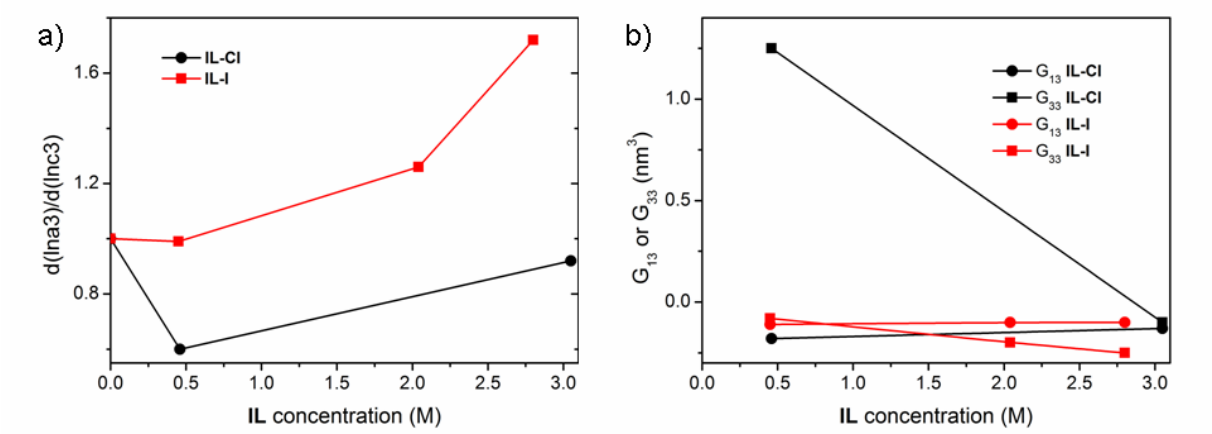

Figure S7. a) The non-ideality of the solution is displayed in activity derivative coefficient, a_{33}, evaluated *via* equation S2, again as a function of **IL** concentration. b) Kirkwood-Buff integrals derived from $g_{33}=g_{\mathbf{IL\text{-}IL}}$ and $g_{31}=g_{\mathbf{IL}\text{-solvent}}$ in Figure S4, and S5 according to equation S1. Variation of integrals with **IL** concentration for **IL-Cl** (black) and **IL-I** (red) are compared. All curves are obtained from simulations at 300 K.

Figure S7 provides another thermodynamic view on the **IL-Cl** and **IL-I** systems, here in terms of the activity coefficient derivative a_{33} of **IL** (Equation S2). This coefficient is below 1 for **IL-Cl**, and above 1 for **IL-I**. From the integration of a_{33} it follows that activity coefficient of **IL**, a_3, is above 1 for **IL-I**, but below 1 for **IL-Cl**.

As found recently,[S12,13] the effective potential, $u_{eff}(r)$, can be decomposed into specific short range, $u^{sr}_{eff}(r)$, and nonspecific electrostatic long range, $u^{sc}_{eff}(r)$, contributions (i.e., screened Coulomb interaction) in certain cases (see equation S5). Up to molar concentrations, this approach allows to approximately evaluate the second virial coefficient, through its particular concentration dependent form (equation S6).[S13]

$$u^{sr}_{eff}(r) = u_{eff}(r;c_3) - u^{sc}(r;c_3) \quad (eq.S5)$$

$$\beta P = c_3 + B_2(T;c_3)c_3^2 + B_3c_3^3 = c_3 + \left(B_2^{sr}(T) + B_2^{sc}(T;c_3)\right)c_3^2 + B_3c_3^3 \quad (eq.S6)$$

Unfortunately, the concentration ranges of the **IL**/acetone demixing process were too high to directly apply the above mentioned approach.

We have studied the concentration and temperature effect on the structures of 1,3-dimethylimidazolium iodide and chloride. We focus on the local solution structure near the 1,3-dimethylimidazolium, in particular the height of peaks in g(r)s (strength of association), and its variation with temperature and with concentration of ionic-liquid. We find that the observed trends for **IL-I** allow for the observation of LCST, *i.e.*, the ion-pairing is strengthened with temperature and rather insensitive to increased concentration. In contrast, the trends (temperature and concentration dependences of solution structure) observed with chloride are unlikely to allow for LCST phase behavior.

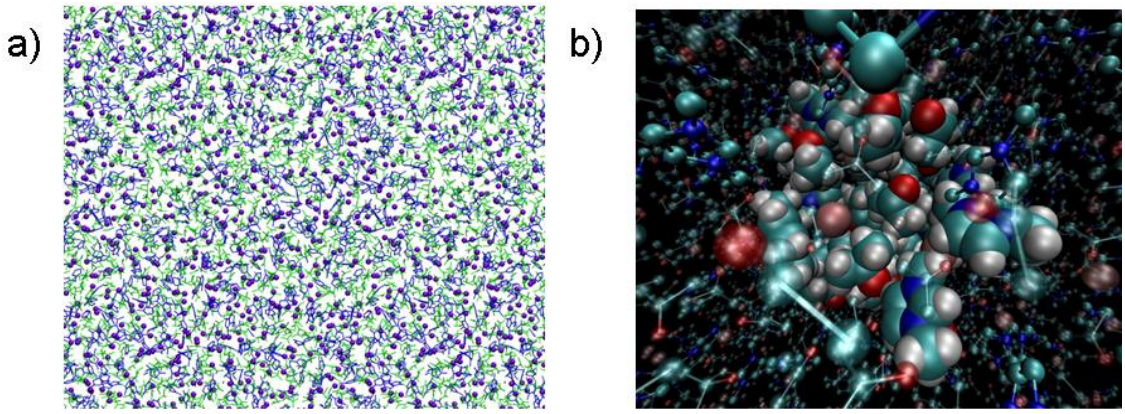

Figure S8: (a) The global (acetone green, 1,3-dimethylimidazolium cation blue, and iodide violet) and (b) local (iodide pink and 1,3-dimethylimidazolium blue and cyan) snapshot of the 1,3-dimethylimidazolium iodide: acetone solution after 100 ns of the simulation (at 300K, and **IL-I** concentration 1170 mg/mL). Clearly, no clustering occurs, neither on the global nor the local scale.

At high ionic liquid concentration (1170 mg/mL, ~ $x_{\mathbf{IL}}$ = 0.27), the solution is fairly homogeneous on a global scale with transient clustering only on the local scale. This is documented in Figure S8, where we show a snapshot after 100 ns of MD simulation at 300 K

7. References

S1 C. Li, L. Zhao, J. Li, X. Ding, S. Chen, Q. Zhang, Y. Yu, X. Jia, *Chem. Commun.* **2010**, *46*, 9016–9018.

S2 S. Dong, B. Zheng, Y. Yao, C. Han, J. Yuan, M. Antonietti, F. Huang, *Adv. Mater.* 2013, **25**, 6864–6867.

S3 J. Schmidt, C. Krekeler, F. Dommert, Y. Zhao, R. Berger, L. Delle Site, C. Holm, *J. Phys. Chem. B* 2010, **114**, 6150–6155.

S4 J. N. Canongia Lopes, A. A. H. Pádua, *J. Phys. Chem. B* 2006, **110**, 19586–19592.

S5 C. Caleman, P. J. van Maaren, M. Hong, J. S. Hub, Costa, L. T.; D. van der Spoel, *J. Chem. Theory Comput.* 2012, **8**, 61–74.

S6 D. Van der Spoel, E. Lindahl, B. Hess, G. Groenhof, A. E. Mark, H. J. C. Berendsen, *J. Comput. Chem.* 2005, **26**, 1701–1718.

S7 G. Bussi, D. Donadio, M. Parrinello, *J. Chem. Phys.* 2007, **126**, 014101.

S8 M. Parrinello, A. Rahman, *J. Appl. Phys.* 1981, **52**, 7182–7190.

S9 J. G. Kirkwood, F. P. Buff, *J. Chem. Phys.* 1951, **19**, 774–777.

S10 V. Pierce, M. Kang, M. Aburi, S. Weerasinghe, P. E. Smith, *Cell Biochem. Biophys.* 2008, **50**, 1–22.

S11 M. Reinhardt, J. Dzubiella, M. Trapp, P. Gutfreund, M. Kreuzer, A. H. Groeschel, A. H. E. Mueller, M. Ballauff, R. Steitz, *Macromolecules* 2014, **46**, 6541–6547.

S12 J. Heyda, M. Lund, M. Oncak, P. Slavicek, P. Jungwirth, *J. Phys. Chem. B* 2010, **114**, 10843–10852.

S13 I. Kalcher, J. Dzubiella, *J. Chem. Phys.* 2009, **130**, 134507.